No. 128/23, 33–56
ISSN 2657-6988 (online)
ISSN 2657-5841 (printed)
DOI: 10.26408/128.03

Submitted: 24.10.2023
Accepted: 16.11.2023
Published: 29.12.2023

KINEMATIC AND DYNAMICS MODELING OF NONHOLONOMIC MOBILE ROBOT

Krzysztof Jasiński[1], Lech Murawski[2], Adam Szeleziński*[3], Marcin Kluczyk[4]

[1] Gdynia Maritime University, 81-87 Morska St., 81-225 Gdynia, Poland, Faculty of Electrical Engineering

[2, 3] Gdynia Maritime University, 81-87 Morska St., 81-225 Gdynia, Poland, Faculty of Maritime Engineering

[4] Polish Naval Academy of the Heroes of Westerplatte, 69 Śmidowicza St., 81-127 Gdynia, Poland, Faculty of Mechanical and Electrical Engineering

[1] k.jasinski@we.umg.edu.pl, ORCID 0000-0001-8355-6167

[2] l.murawski@wm.umg.edu.pl, ORCID 0000-0003-0089-5492

[3] a.szelezinski@wm.umg.edu.pl, ORCID 0000-0003-2842-0683

[4] m.kluczyk@amw.gdynia.pl, ORCID 0000-0001-7357-6762

*Corresponding author

Abstract: This paper presents computer simulation results of kinematic and dynamic of two and three – wheeled mobile robot, conducted in the Matlab&Simulink packet environment. Models of kinematics and dynamics were developed with the aid of Jacobians and Lagrange II multiplayers equations.

Keywords: robotics, modeling, control, mechatronics.

1. INTRODUCTION

The problem of describing the kinematics and dynamics of mobile robots has already been the subject of many scientific papers [Żylski 1996; Jasiński 2004; Mazur 2010; Giergiel, Hendzel and Żylski 2013; Kaliński and Mazur 2016a,b]. Nevertheless, simplifications that are difficult to substantiate are still used when describing kinematics and dynamics. In most of the works in this area, no attempt has been made to assess the impact of these simplifications on the correctness of the synthesis of the control system of mobile robots.

2. DESCRIPTION OF MOBILE ROBOT CIRCULAR MOTION KINEMATICS

Mobile wheeled robots are mostly systems with two degrees of freedom. In practice, three-wheeled and four-wheeled mobile robot designs are most common. In describing the kinematics of such systems, it does not matter how many driving wheels are present in the system – the methodology for describing the motion and the way models are developed should be similar. However, observing the solutions of the developed computational models for mobile robots with different 34umer of wheels (either equipped with steering or not), it is possible to notice differences in their behaviour when driving along the same trajectory.

3. METHODS OF DESCRIPTION

When describing the kinematics of wheeled mobile robots, the most common equations of kinematics are given, in the form of which homogeneous coordinates and transformation matrices (homogeneous transformation) are used to determine them [Giergiel, Hendzel and Żylski 2013]. After making the basic assumption that there are no slips in the system, the kinematics equations of the characteristic points of the robot system are determined. Since nonholonomic constraints are imposed on the system analysed, the equations of these constraints are given as a linear system of equations with respect to velocity. The analysis of the kinematics of the motion of mobile wheeled robots, usually involves solving the so-called "inverse kinematics task" [Żylski 1996].

This solution is based on the assumption that the selected characteristic point of the mobile robot system moves along a specific motion trajectory (e.g. circular). At the same time, it is assumed that the value of the velocity of motion of another characteristic point of the robot system is known. Solving these equations of kinematics makes it possible to formulate guidelines for the correct construction of the trajectory of motion of the selected point, taking into account the requirements for speed and travel time of the system analysed.

4. KINEMATICS OF A TWO-WHEELED MOBILE ROBOT

The robot's driving system consists of two front driving wheels 2 and 3 and a rear trailing wheel 4 (Fig. 1). The driving wheels do not change their position in relation to the robot frame 1. Movement along an arc of radius R of the robot analysed is possible as a result of appropriate control of the speeds of the driving wheels.

Torsion of the trailing wheel 4 occurs automatically, due to a change in the speed of the driving wheels. The angle of twist of the trailing wheel in relation to the

frame depends on the geometry of the robot system, i.e. the radius of the arc *R*. It is assumed that the speed of the characteristic point *A*, which belongs to the frame 1, is known. Also attached to the robot frame is an inductive sensor, which tracks the trajectory along which the robot moves, shown in the figure as the characteristic point *E*. It is thanks to the information obtained from the inductive sensor that the robot performs the set trajectory of movement (so-called inductive planning lines).

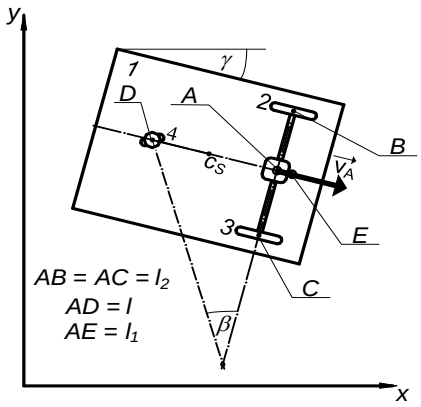

Fig. 1. Model of a two-wheeled mobile robot

Source: own elaboration.

The mathematical model of a two-wheeled mobile robot is given by a system of equations (1):

$$\begin{cases} \dot{\beta} = \dfrac{v_A}{R \cdot \cos(\beta - \gamma)}, \\ \dot{\gamma} = \dfrac{v_A \cdot tg(\beta - \gamma)}{l_1}, \\ \dot{\alpha}_1 = \dfrac{v_A}{r} + \dot{\gamma} \cdot \dfrac{l_2}{r}, \\ \dot{\alpha}_2 = \dfrac{v_A}{r} - \dot{\gamma} \cdot \dfrac{l_2}{r}, \\ \dot{\alpha}_3 = \dfrac{\sqrt{v_A{}^2 + (\dot{\gamma} \cdot l)^2}}{r_2}. \end{cases} \tag{1}$$

where:

γ – the instantaneous angle of rotation of the frame 1,
β – the instantaneous angle of rotation on the circular track,
$\dot{\gamma}$ – instantaneous γ angle velocity change,
$\dot{\beta}$ – instantaneous angular velocity of the characteristic point *E* (at this point the sensor that controls the track is located),
$\dot{\alpha}_1$ – instantaneous angular velocity of driving wheel 2,
$\dot{\alpha}_2$ – instantaneous angular velocity of driving wheel 3,
$\dot{\alpha}_3$ – instantaneous angular velocity of trailing wheel 4,
v_A – speed of the characteristic point *A*,
R – radius of the arc along which point *E* moves,
l_1 – the distance between point *A* and point *E*,
l_2 – the distance between point *A* and the point of contact of the driving wheel with the surface on which robot *B* or *C* moves,
l – the distance between the axis of the driving wheels and the axis of the trailing wheel,
r – the radius of the driving wheels,
r_2 – the radius of the trailing wheel.

5. KINEMATICS OF A THREE-WHEELED MOBILE ROBOT

Figures 2 and 3 show a model of a three-wheeled mobile robot. The basic assemblies of the above model are frame 1, drive system *UN* and steering system *UK*. The drive train consists of wheels 2 and 3, which are mounted on drive half-shafts. The wheels are set into rotary motion via a set of gears and drive half-shafts by an electric motor. The proper rotational speeds of wheels 2 and 3 during curve travel are provided by the differential, which, together with the transmission assembly, is called the drive bridge.

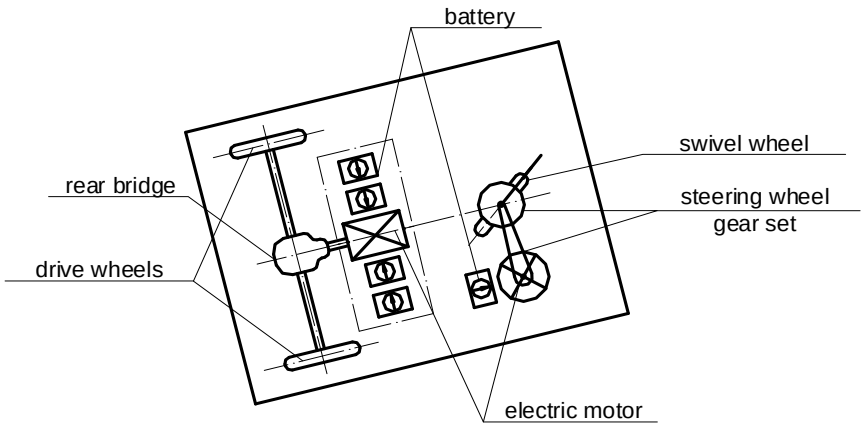

Fig. 2. Model of the drive system and power system of a three-wheeled mobile robot

Source: own elaboration.

Wheels 2 and 3 rotate about their own axes, which do not change position relative to the frame 1. The steering system consists of a steering wheel 5, which is turned by an electric motor and gear set (it rotates relative to a vertical axis bearing in the frame), and a wheel 4, which is free to rotate relative to the axis bearing in the steering wheel.

Typically, the wheels cooperating with the roadway found in a mobile wheeled robot system are not equipped with tires, but with metal discs coated with a layer of rubber. The radii of all wheels are the same and have a value of *r*.

The equations describing the kinematics of the three-wheeled mobile robot are of the form:

$$\begin{cases} \dot{\beta} = \dfrac{\cos(\gamma+\varphi)\cdot\cos\gamma}{R\cdot\sin(\gamma+\varphi)\cdot\sin\beta + R\cdot\cos(\gamma+\varphi)\cdot\cos\beta}\cdot v_A + \dfrac{\sin(\gamma+\varphi)\cdot\sin\gamma}{R\cdot\sin(\gamma+\varphi)\cdot\sin\beta + R\cdot\cos(\gamma+\varphi)\cdot\cos\beta}\cdot v_A + \\ + \dfrac{\sin(\gamma+\varphi)\cdot\cos\gamma\cdot tg\varphi - \cos(\gamma+\varphi)\cdot\sin\gamma\cdot tg\varphi}{R\cdot\sin(\gamma+\varphi)\cdot\sin\beta + R\cdot\cos(\gamma+\varphi)\cdot\cos\beta}\cdot v_A \\ \dot{\gamma} = \dfrac{v_A\cdot tg\gamma}{l}, \\ \dot{\varphi} = \dfrac{\sin\beta\cdot\cos\gamma}{l_3\cdot\sin(\gamma+\varphi)\cdot\sin\beta + l_3\cdot\cos(\gamma+\varphi)\cdot\cos\beta}\cdot v_A - \dfrac{\cos\beta\cdot\sin\gamma}{l_3\cdot\sin(\gamma+\varphi)\cdot\sin\beta + l_3\cdot\cos(\gamma+\varphi)\cdot\cos\beta}\cdot v_A + \\ + \dfrac{-l\cdot\sin\gamma\cdot\sin\beta\cdot tg\varphi - l_3\cdot\sin(\gamma+\varphi)\cdot\sin\beta\cdot tg\varphi - l\cdot\cos\gamma\cdot\cos\beta\cdot tg\varphi - l_3\cdot\cos(\gamma+\varphi)\cdot\cos\beta\cdot tg\varphi}{l\cdot l_3\cdot\sin(\gamma+\varphi)\cdot\sin\beta + l\cdot l_3\cdot\cos(\gamma+\varphi)\cdot\cos\beta}\cdot v_A \\ \dot{\alpha}_2 = \dfrac{v_A}{r} - \dot{\gamma}\cdot\dfrac{l_2}{r}, \\ \dot{\alpha}_3 = \dfrac{v_A}{r} + \dot{\gamma}\cdot\dfrac{l_2}{r}, \\ \dot{\alpha}_4 = \dfrac{v_A}{r}\cdot\dfrac{\cos\gamma}{\cos(\gamma+\varphi)} - \dot{\gamma}\cdot\dfrac{l}{r}\cdot\dfrac{\sin\gamma}{\cos(\gamma+\varphi)}. \end{cases} \tag{2}$$

6. METHODOLOGY FOR DESCRIBING THE DYNAMICS OF A MOBILE ROBOT CIRCULAR MOTION

When describing the dynamics of motion of mobile wheeled robots, an analysis of the motion of the system on which nonholonomic constraints are imposed is carried out. Starting this description, it is necessary to simplify the existing robot model, adopted for the purpose of describing the kinematics [Giergiel, Hendzel and Żylski 2013]. Typically, a so-called surrogate model is built, in which, instead of three or four real wheels (or more), there are two so-called surrogate wheels. Thus, in the case of a three-wheeled mobile robot model, consisting of two rear driving wheels and one front turning wheel, a model is created in which the two driving wheels are replaced by one wheel, placed at a specific point in the model. The choice of this point should, allow easy determination of the kinematic parameters of the substitute

wheel, based on the previous solution of the kinematic model with two driving wheels. When building a surrogate model for such a three-wheeled robot, it is not necessary to change the previous assumptions for the front steering wheel.

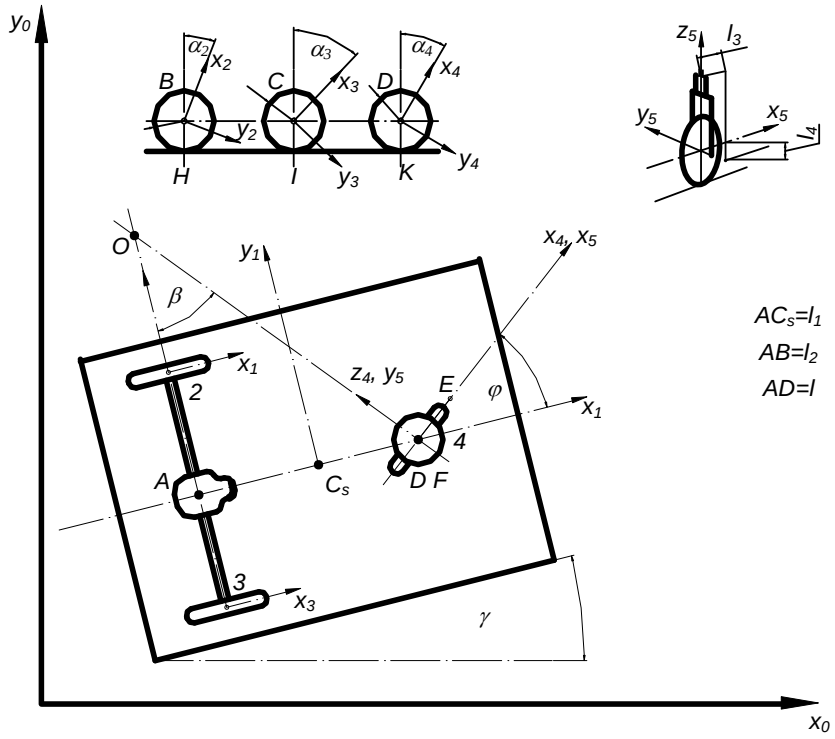

Fig. 3. Model of a three-wheeled mobile robot

Source: own elaboration.

Regardless of the number of wheels, it is advantageous and expedient to introduce a model where only two wheels are present. Practically, ideally, one wheel should be the driving wheel to which the torque from the driving motor is applied, and the other wheel should be the steering wheel to which the torque from the motor driving the system is applied [Żylski 1996].

In the case where we are analysing the dynamics of a mobile wheeled robot whose chassis consists of four non-torsion driving wheels, we replace the front driving wheels with one so-called "surrogate wheel" as well as model the rear wheels with a second surrogate wheel. Once the surrogate model is acquired, we modify the existing constraint equations defined for the model describing the kinematics of the mobile robot to a form that can be used to solve the dynamics of the system under study. To do this, we need, among other things, to determine the generalised coordinate vector, taking into account the angular velocity of the surrogate wheels,

and to determine the relationship between the angular velocities of the real wheels and the angular velocity of the surrogate wheel. Only at the end of the existing constraint equations do we present the vector in a form that takes into account the "new" generalised coordinates.

In this work, Lagrange equations were used to describe the movement of the model, in which

$$\frac{d}{dt}\left(\frac{\partial \mathbf{E}}{\partial \dot{\mathbf{q}}^{j}}\right)-\frac{\partial \mathbf{E}}{\partial \mathbf{q}^{j}}=\mathbf{Q}_{j}+\sum_{\nu=1}^{l_r}\lambda_{\nu}^{(2)}\cdot \mathbf{C}_{\nu j}^{(2)}, \tag{3}$$

where:

- $\mathbf{E}$ – kinetic energy of the individual components of the robot when traveling along a specified trajectory,
- $\mathbf{q}$ – vector of generalized coordinates,
- $\mathbf{Q}_j$ – vector of generalized forces,
- $\mathbf{C}_{vj}^{(2)}$ – function of generalized coordinates and time,
- $\lambda_{vj}^{(2)}$ – Lagrange multipliers.

The left-hand side of the Lagrange equation is formed by determining the kinetic energy of the individual elements that make up the system analysed. Both the kinetic energy of progressive and rotational motion of the robot elements are taken into account.

In determining the generalised forces occurring on the right side of the Lagrange equation, the torque driving the wheel in question and the torque controlling the torsion of the corresponding wheel are taken into account. The resistance to motion occurring when the wheels roll or turn is also taken into account. Typically, individual wheels are driving, or turned, by separate motors. For this reason, the values of the moments applied to these wheels when travelling along a given trajectory cannot be arbitrary. It is therefore necessary to provide additional equations describing the distribution of power in the drive system.

The multipliers occurring in the Lagrange equations describe the values of the dry friction forces lying in the plane of contact of the substitute wheels. One common assumption is that there is no slippage between the wheels of the mobile robot and the ground on which it moves. This assumption means that the angular velocities of rotation around the axis of the driving wheels, as well as the angular velocities of turning of the corresponding wheels, cannot be arbitrary.

When deriving the equations describing the movement of wheeled mobile robots, it is also useful to know the values of the contact forces of the wheels on the surface. The forces of interaction, of the road surface on the wheels (or the wheels on the road), can be determined from equations derived from static or kinetostatic equilibrium [Żylski 1996].

The mathematical model obtained as a result of the derivation, should consist of differential equations of motion that uniquely describe the movement of a mobile wheeled robot. The number of these equations corresponds to the sum, the number of degrees of freedom of the system and the number of constraint equations specified for the system in question [Giergiel, Hendzel and Żylski 2013].

Once the differential equations showing the motion of the mobile robot are obtained, it is possible to analyse the task of simple and inverse dynamics. When modelling the dynamics of the same system, it is possible to determine the values of the driving and torsional moments of the corresponding wheels. This is the so-called inverse dynamics task. Due to the very complex form of the differential equations of motion of a mobile robot, their solution is very difficult.

In such a situation, it is necessary to introduce transformations decoupling Lagrange multipliers from moments. As a result of such an action, the differential equations of motion in the so-called reduced form with nonholonomic bonds are obtained. The detailed method of carrying out this transformation, is presented in the work [Giergiel, Hendzel and Żylski 2013].

Knowledge of the reduced differential equations of motion greatly simplifies, the procedure for determining the driving and torsional moments of the corresponding wheels, and makes it possible to determine the value of the dry friction forces between the wheels and the surface on which the robot moves.

7. DYNAMICS OF A THREE-WHEELED MOBILE ROBOT

On the basis of the described methodology, an equivalent model of the three-wheeled mobile robot was developed (Fig. 4), and differential equations of motion describing the dynamics of the three-wheeled mobile robot were derived from the solution, the so-called "inverse dynamics task".

Figure 4 shows the three-wheeled robot model adopted for the dynamics analysis. Wheels 2 and 3 of the model presented in Figures 2 and 3 have been replaced by a single substitute wheel 2*z* with its centre at the characteristic point *A*. It was also assumed that we continue to analyse the movement of the robot along the trajectory determined by the movement of the characteristic point *E* and that the angle of rotation of its own substitute wheel *2z*, describes the angle ψ:

$$\begin{aligned} \psi &= \alpha_2 - \frac{r \cdot \gamma}{l_2}, \\ \psi &= \alpha_3 + \frac{r \cdot \gamma}{l_2}. \end{aligned} \tag{4}$$

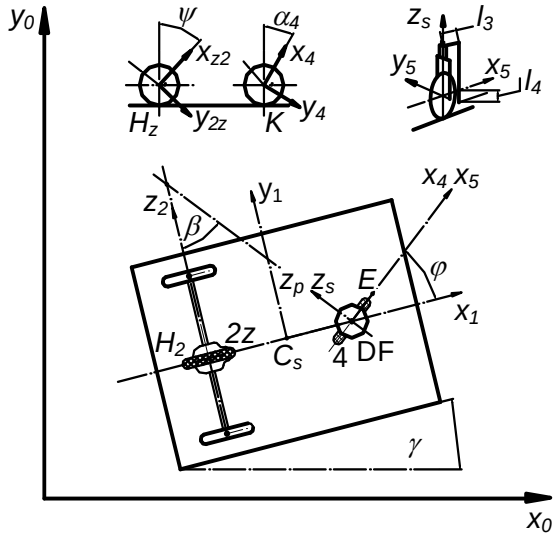

Fig. 4. Equivalent model of a three-wheeled mobile robot

Source: own elaboration.

The angle of rotation of the torsion wheel's own 4, is denoted in the same way as when solving the kinematics problem as α_4.

The vector of generalized coordinates, for the surrogate model thus adopted, will be of the form:

$$\mathbf{q}^j = \begin{bmatrix} x_A \\ y_A \\ \gamma \\ \alpha_4 \\ \psi \\ \varphi \end{bmatrix}, \tag{5}$$

After performing mathematical operations according to the methodological description presented, we obtain the differential equations of motion for the mobile robot, described by the following system of equations, in which:

$$
\begin{cases}
(m_1 + 2\cdot m_2 + m_4)\cdot \ddot{x}_A - (m_1\cdot l_1 + m_4\cdot l)\cdot\left[(\ddot{\gamma})\cdot\sin\gamma + (\dot{\gamma})^2\cdot\cos\gamma\right] = \lambda_1 + \lambda_3, \\
(m_1 + 2\cdot m_2 + m_4)\cdot \ddot{y}_A + (m_1\cdot l_1 + m_4\cdot l)\cdot\left[(\ddot{\gamma})\cdot\cos\gamma - (\dot{\gamma})^2\cdot\sin\gamma\right] = \lambda_2 + \lambda_4, \\
\left[m_1\cdot(l_1)^2 + 2\cdot m_2\cdot(l_2)^2 + m_4\cdot(l)^2\right]\cdot\ddot{\gamma} + (m_1\cdot l_1 + m_4\cdot l)\cdot(-\ddot{x}_A\cdot\sin\gamma + \ddot{y}_A\cdot\cos\gamma) + \\
+\left[I_{z1} + 2\cdot I_{z2}\cdot\left(\frac{r}{l_2}\right)^2 + 2\cdot I_{x2} + I_{x4}\right]\cdot\ddot{\gamma} + I_{x4}\cdot\ddot{\varphi} = \lambda_3\cdot l\cdot\sin\gamma + \lambda_4\cdot l\cdot\cos\gamma + \\
+ M_s + M_o\cdot\operatorname{sgn}\varphi, \\
I_{z2}\cdot\ddot{\alpha}_4 = -\lambda_3\cdot r\cdot\cos(\gamma+\varphi) - \lambda_4\cdot r\cdot\sin(\gamma+\varphi) - \left(m_4 + \frac{m_1}{2}\right)\cdot g\cdot f, \\
2\cdot I_{z2}\cdot\ddot{\psi} = -\lambda_1\cdot r\cdot\cos\gamma - \lambda_2\cdot r\cdot\sin\gamma - \left(2\cdot m_2 + \frac{m_1}{2}\right)\cdot g\cdot f.
\end{cases}
\tag{6}
$$

where:

- m_1 – mass of robot frame 1,
- m_2 – mass of driving wheels 2 or 3,
- m_4 – mass of torsion wheel 4, including steering wheel 5,
- l – distance between axis of driving wheels 2 and 3 and axis of torsion wheel 4,
- l_1 – distance between characteristic point A and center of gravity of robot frame 1 point c_s,
- l_2 – distance between point *A* and the point of tangency of driving wheels with roadway,
- I_{x2} – moment of inertia of driving wheels, relative to axis *x*,
- I_{x4} – moment of inertia of torsion wheel 4 with respect to axis *x*,
- I_{z1} – moment of inertia of robot frame *1* with respect to axis *z*,
- I_{z2} – moment of inertia of driving wheels with respect to axis *z* (it was also assumed that the moment of inertia of torsion wheel has the same value $I_{z1} = I_{z4}$),
- r – radius of driving and torsion wheels,
- f – coefficient of rolling friction of wheels with roadway,
- g – acceleration of the Earth,
- M_o – moment of resistance in the friction pair wheel – roadway,
- M_s – torsional moment of wheel 4,
- M_n – driving moment acting on wheels 2 and 3.

The differential equations of motion of the mobile robot, presented in the form of expression (6), have an entangled form. That is, the right side of these equations is complicated and makes solving them much more difficult. In such a situation, a transformation that decouples Lagrange multipliers from moments is applied to systems with nonholonomic bonds. These operations make it possible to obtain differential equations of motion in the so-called reduced form, the solution of which is much easier (7).

$$
\begin{cases}
M_s = \dfrac{I_{x4}\cdot r\cdot\ddot{\psi}\cdot tg\varphi}{l} + I_{x4}\cdot\ddot{\varphi} + \dfrac{I_{x4}\cdot r\cdot\dot{\psi}\cdot\dot{\varphi}}{l\cdot\cos^2\varphi} + M_o\cdot\operatorname{sgn}\dot{\varphi}, \\
M_n = \left[\left(m_1+2\cdot m_2+m_4\right)\cdot r^2 + I_{z2}\cdot\left(2+\dfrac{1}{\cos^2\varphi}\right)\right]\cdot\ddot{\psi} + \dfrac{I_{x4}\cdot r\cdot\ddot{\varphi}\cdot tg\varphi}{l} + \dfrac{\ddot{\psi}\cdot r^2\cdot tg^2\varphi}{l^2}\cdot \\
\cdot\left[I_{z1}+2\cdot I_{z2}\cdot\left(\dfrac{r}{l_2}\right)^2 + 2\cdot I_{x2} + I_{x4} + m_1\cdot\left(l_1\right)^2 + 2\cdot m_2\cdot\left(l_2\right)^2 + m_4\cdot l^2\right] + \\
+\left\{\left[I_{z1}+2\cdot I_{z2}\cdot\left(\dfrac{r}{l_2}\right)^2 + 2\cdot I_{x2} + I_{x4} + m_1\cdot\left(l_1\right)^2 + 2\cdot m_2\cdot\left(l_2\right)^2 + m_4\cdot l^2\right]\cdot\dfrac{r^2}{l^2} + I_{z2}\right\}\cdot \\
\cdot\dfrac{\dot{\varphi}\cdot\dot{\psi}\cdot tg\varphi}{\cos^2\varphi} + \left[\left(2\cdot m_2+\dfrac{m_1}{2}\right)+\left(m_4+\dfrac{m_1}{2}\right)\cdot\dfrac{1}{\cos\varphi}\right]\cdot g\cdot f - \dfrac{I_{x4}\cdot r^2\cdot\ddot{\psi}\cdot tg^2\varphi}{l^2} - \\
- I_{x4}\cdot tg\varphi\cdot\dfrac{r}{l}\cdot\ddot{\varphi} - \dfrac{I_{x4}\cdot tg\varphi\cdot r^2\cdot\dot{\psi}\cdot\dot{\varphi}}{l^2\cdot\cos^2\varphi}, \\
\lambda_4 = \left(\dfrac{1}{l\cdot\cos\gamma + l\cdot\sin\gamma\cdot tg\left(\gamma+\varphi\right)}\right)\cdot \\
\cdot\left\{\left[I_{z1}+2\cdot I_{z2}\cdot\left(\dfrac{r}{l_2}\right)^2 + 2\cdot I_{x2} + I_{x4} + m_1\cdot\left(l_1\right)^2 + 2\cdot m_2\cdot\left(l_2\right)^2 + m_4\cdot l^2\right]\cdot\right. \\
\cdot\left(\ddot{\psi}+\dfrac{r\cdot\dot{\psi}\cdot\dot{\varphi}}{l\cdot\cos^2\varphi}\right) + I_{x4}\cdot\ddot{\varphi} + \left(m_1\cdot l_1 + m_4\cdot l\right)\cdot\dfrac{r^2}{l}\cdot\left(\dot{\psi}\right)^2\cdot tg\varphi - M_s + M_o\cdot\operatorname{sgn}\dot{\varphi} - \\
\left. - \dfrac{l\cdot\left(m_4+\dfrac{m_1}{2}\right)\cdot g\cdot f\cdot\sin\gamma}{r\cdot\cos\left(\gamma+\varphi\right)} - \dfrac{I_{z2}\cdot\ddot{\psi}\cdot l\cdot\sin\gamma}{r\cdot\cos\varphi\cdot\cos\left(\gamma+\varphi\right)} - \dfrac{I_{z2}\cdot\dot{\psi}\cdot\dot{\varphi}\cdot\sin\varphi\cdot l\cdot\sin\gamma}{r\cdot\cos^2\varphi\cdot\cos\left(\gamma+\varphi\right)}\right\}, \\
\lambda_3 = -\dfrac{\left(m_4+\dfrac{m_1}{2}\right)\cdot g\cdot f}{r\cdot\cos\left(\gamma+\varphi\right)} - \dfrac{I_{z2}\cdot\ddot{\psi}\cdot l\cdot\sin\gamma}{\cos\varphi\cdot r\cdot\cos\left(\gamma+\varphi\right)} - \dfrac{I_{z2}\cdot\dot{\psi}\cdot\dot{\varphi}\cdot\sin\varphi\cdot l\cdot\sin\gamma}{\cos^2\varphi\cdot r\cdot\cos\left(\gamma+\varphi\right)} - \\
- \lambda_4\cdot tg\left(\gamma+\varphi\right), \\
\lambda_2 = \left(m_1+2\cdot m_2+m_4\right)\cdot r\cdot\left[\ddot{\psi}\cdot\sin\gamma + \dfrac{r}{l}\cdot\left(\dot{\psi}\right)^2\cdot tg\varphi\cdot\cos\gamma\right] + \left(m_1\cdot l_1 + m_4\cdot l\right)\cdot \\
\cdot\dfrac{r}{l}\cdot\left[\ddot{\psi}\cdot tg\varphi\cdot\cos\gamma - \dfrac{r}{l}\cdot\left(\dot{\psi}\right)^2\cdot tg^2\varphi\cdot\sin\gamma + \dot{\psi}\cdot\dot{\varphi}\cdot\dfrac{\sin\gamma}{\cos^2\varphi}\right] - \lambda_4, \\
\lambda_1 = \left(m_1+2\cdot m_2+m_4\right)\cdot r\cdot\left[\ddot{\psi}\cdot\cos\gamma + \dfrac{r}{l}\cdot\left(\dot{\psi}\right)^2\cdot tg\varphi\cdot\sin\gamma\right] - \left(m_1\cdot l_1 + m_4\cdot l\right)\cdot \\
\cdot\dfrac{r}{l}\cdot\left[\ddot{\psi}\cdot tg\varphi\cdot\sin\gamma + \dfrac{r}{l}\cdot\left(\dot{\psi}\right)^2\cdot tg^2\varphi\cdot\cos\gamma + \dot{\psi}\cdot\dot{\varphi}\cdot\dfrac{\sin\gamma}{\cos^2\varphi}\right] - \lambda_3.
\end{cases}
\tag{7}
$$

The solution of the system of differential equations describing the motion of a mobile robot makes it possible to determine, among other things, the driving moments and the torsional moment. Knowledge of these values is needed in the design of the executive systems of real mobile robot systems, as well as in the synthesis of algorithms for controlling the tracking motion of these units. Knowledge of Lagrange multipliers and frictional forces, makes it possible to assess whether one of the basic assumptions made during the "construction" of the mathematical model – that there is no slippage between the wheel and the roadway – is met, given the given motion parameters (travel speed).

8. PARAMETERS AND COURSE OF SIMULATION

The research consisted in simulating the kinematic model in Matlab & Simulink, given by the system of equations (2), and the dynamic model, described by the system of equations (7), of the three-wheeled mobile robot. In addition, a simulation was performed - for comparison of the obtained results - of the kinematic model of the two-wheeled mobile robot Pioneer-2DX. For this purpose, the computational model given by equation (1) was used.

Simulations of both the two-wheeled and three-wheeled robot involved solving the inverse task of kinematics and the inverse task of dynamics.

Figure 5 shows the planned motion trajectory of the characteristic point *E*.

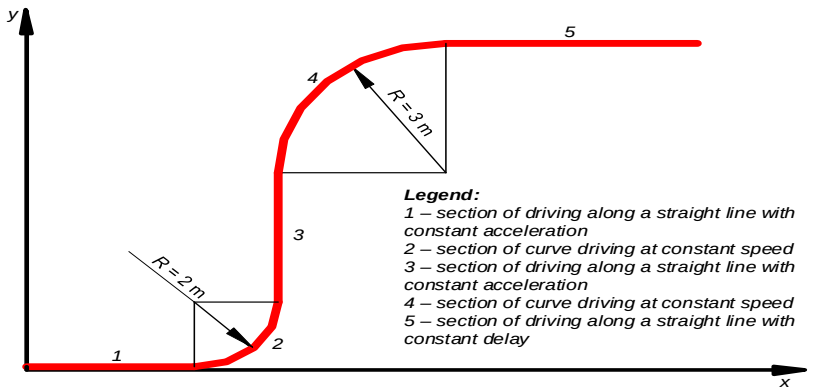

Fig. 5. The trajectory of motion of the characteristic point *E*

Source: own elaboration.

The motion trajectory of point *E* consists of a rectilinear section, on which the robot accelerates to reach the set speed, and a curve with a radius of $R = 2$ [m], on which it maintains a constant speed. After exiting the curve, point *E* again travels along the rectilinear section and the robot accelerates again, and then enters the curve

again, this time with a radius of $R = 3$ [m], reaching a speed twice that of the beginning of the ending rectilinear section. As the robot travels around the curve, it again maintains a constant speed. The trajectory ends with a rectilinear section, where braking begins until the robot stops.

Table 1 lists the values of the coefficients, which determine the geometry of the system under analysis, as well as the masses and mass moments of inertia of the three-wheeled mobile robot. These constants are necessary for solving the systems of equations (2), and (7). The adopted values of the coefficients are consistent with those determined from the study of the real *Robocar C80* robot [Żylski 1996].

Table 1. Values of constants occurring in the mathematical model of the three-wheeled robot

No.	Name of constant	Symbol	Value	Units
1	Distance between the axis of driving wheels 2 and 3, and the axis of torsion wheel 4	l	0.7	[m]
2	Distance between the characteristic point A and the centre of gravity of robot frame 1 – point C_s	l_1	0.35	[m]
3	Distance between point A and the point of contact of the driving wheel with the surface	l_2	0.35	[m]
4	Distance between characteristic point E and the center of torsion wheel 4	l_3	0.30	[m]
5	The radius of the driving and torsion wheels	r	0.15	[m]
6	The radius of the arc of the trajectory of point E	R	2.0 – 3.0	[m]
7	Speed of the characteristic point A	v_A	0.5 – 1.0	[m/s]
8	Mass of robot frame 1	m_1	980	[kg]
9	Mass of driving wheels 2 and 3	m_2	16	[kg]
10	Mass of torsion wheel 4 with steering wheel 5	m_4	24	[kg]
11	Moment of inertia of driving wheels 2 and 3 relative to axis x	I_{x2}	6	[kg m^2]
12	Moment of inertia of torsion wheel 4 relative to axis x	I_{x4}	10.2	[kg m^2]
13	Moment of inertia of frame 1 relative to axis z	I_{z1}	108	[kg m^2]
14	Moment of inertia of driving wheels 2 and 3, torsion wheel 4 relative to axis z	I_{z2}	2.8	[kg m^2]
15	Moment of resistance in the wheel-roadway friction pair	M_o	40.36	[Nm]
16	Coefficient of rolling friction of driving wheels 2 and 3, torsion wheel 4	f	0.02	[m]
17	Coefficient of sliding friction of driving wheels 2 and 3, torsion wheel 4	μ	0.2	[-]
18	Ratio between driving wheels 2 and 3 and electric motor	i_N	60	[-]
19	Ratio between torsion wheel 4 and electric motor	i_S	120	[-]

Source: own elaboration.

Table 2 gives the values of the coefficients, determining the geometry of the system of the two-wheeled mobile robot analysed and described by the system of equations [Jasiński 2004].

9. SIMULATION RESULTS OF THE THREE-WHEELED ROBOT KINEMATICS

The key to verification of the derived computational model is simulation. Three simulations are presented in this paper. Their presentation includes detailed conditions of the experiment, graphs of the waveforms and conclusions and observations. The results of the simulations were saved in the form of *MAT-files*, and the obtained data saved in *MAT-files* were loaded into Matlab software and then presented in the form of graphs.

Simulation results for the model describing the kinematics of the three-wheeled mobile robot are shown in Figure 6.

Table 2. Values of constants present in the mathematical model of the two-wheeled robot

No.	Name of constant	Symbol	Value	Units
1	Distance between the axis of driving wheels 2 and 3 and the axis of trailing wheel 4	l	0.7	[m]
2	Distance between the characteristic point E and the characteristic point A	l_1	0.20	[m]
3	Distance between point A and the point of contact of the driving wheel with the surface	l_2	0.35	[m]
4	Radius of driving wheels 2 and 3	r	0.15	[m]
5	Radius of trailing wheel 4	r_2	0.05	[m]
6	Radius of the arc of the trajectory of point E	R	2.0 – 3.0	[m]
7	Speed of the characteristic point A	v_A	0.5 – 1.0	[m/s]

Source: own elaboration.

Figure 6a shows the signals at the input and output of the logic block and the value of the angular velocity of the robot characteristic point E. It can be clearly seen that there is a "disturbance" in the signal waveform at the input to the *logic* block. The angle β, between 20 and 22 seconds after the initiation of the simulation, increases its value. This is due to the deliberate generation of an increase in the radius R so as to realise the set trajectory (Fig. 5) and the change in the value of the velocity of point E. The fact of the change in the value of the radius R and velocity v_A at the output of the logic block, is noticeable in the form of a larger angle of the curve.

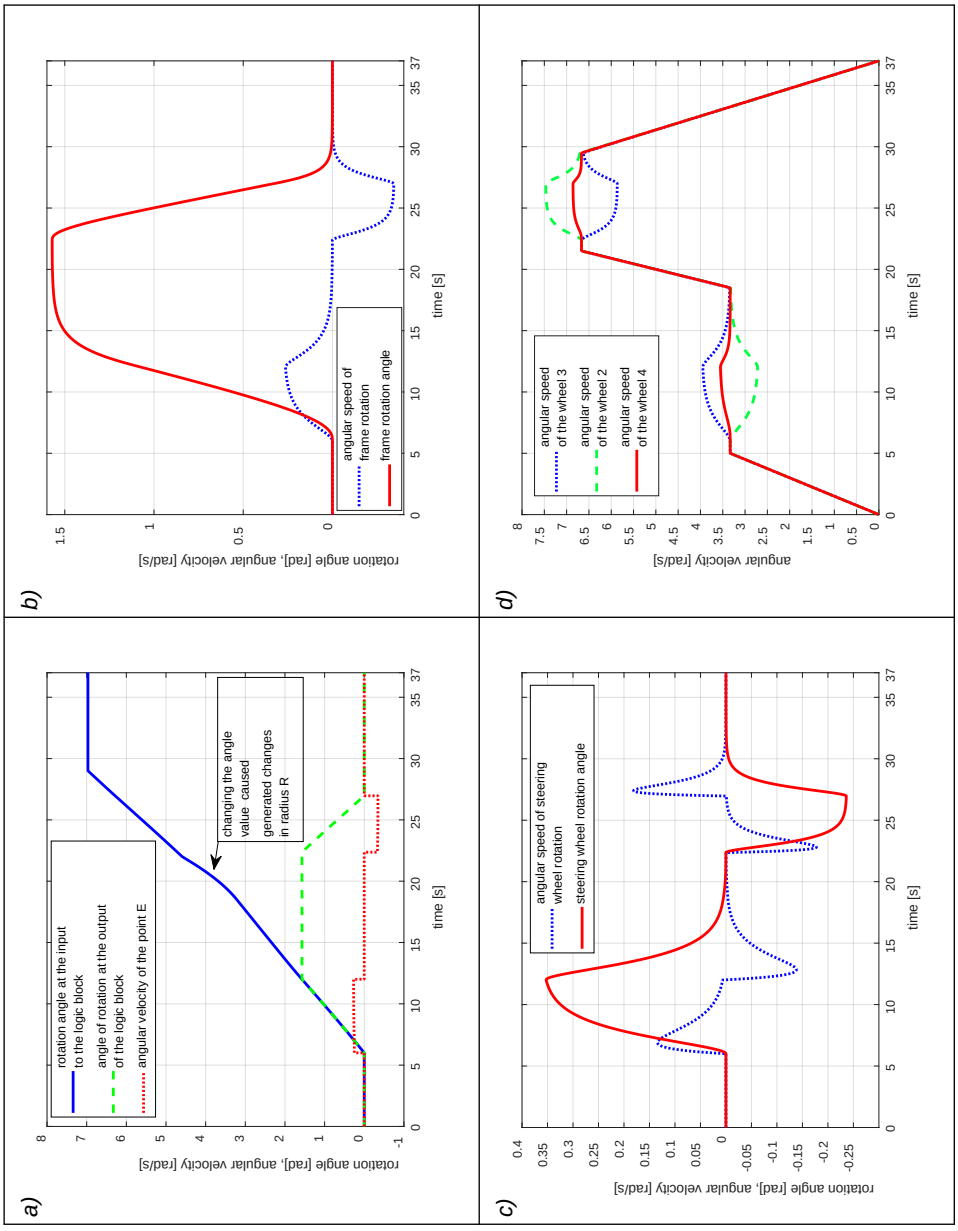

Fig. 6. Simulation results of the kinematic model of a three-wheeled robot: a) changing the instantaneous rotation angle and angular velocity of the robot's characteristic point *E*, b) change in the instantaneous frame rotation angle and the angular speed of frame rotation, c) change in the instantaneous steering angle and its instantaneous angular speed, d) changes in the angular speeds of the robot's wheels

Source: own elaboration.

Figure 6b shows how the angle of instantaneous rotation of frame *1* – γ and its angular velocity – $\dot{\gamma}$ change during the analysed movement of the circular robot. For the first six seconds after the start of the simulation, while the robot is moving along a rectilinear section, the frame rotation angle is 0 [rad]. Then the robot enters a curve with a radius of R = 2 [m], and there is a change in the frame's yaw angle untilit exits the curve at the 18th second after the start of the simulation. Initially, up to the 12th second, the rate of change of the rotation angle increases, reaching a value of 0.263 [rad/s], then decreases to 0 [rad/s] at the exit of the robot from the curve.

A simultaneous analysis of Figures 6a and 6b demonstrates that the rotation angle of the characteristic point E reaches the value $\frac{\pi}{2}$ [rad] after only 12 seconds of simulation and the robot leaves the arc with a radius of R = 2 [m] only after 18 seconds. After traversing the rectilinear section in 22.4 seconds from the start of the simulation, the robot enters the curve again, and this time the robot's movement speed is higher. The arc over which point E moves, is R = 3[m]. The instantaneous angle of rotation of the frame decreases from $\frac{\pi}{2}$ [rad] to 0 [rad] in 7.1 seconds. As before, the speed of the angle change increases at the beginning, up to 0.324 [rad/s], and then decreases to 0 [rad/s] at the exit of the arc.

Figure 6c shows the time course of the change in steering angle *5* – φ and its instantaneous angular velocity $\dot{\varphi}$. When driving on a straight section, the steering wheel is not turned during the first 6 seconds of driving. After entering a curve with a radius of R = 2 [m], the wheels are turned and in the 12th second the steering angle reaches its highest value, equal to 0.353 [rad], after which, in the 18th second, the wheel is straightened and the vehicle travels on a straight section.

The speed of wheel turning is greatest at the beginning of the curve. As early as 6.9 seconds after the start of the simulation, it reaches 0.134 [rad/s], and then it decreases all the time until straightening begins. During the straightening of the twisted wheels, again the speed begins to absolutely "increase," reaching -0.137 [rad/s] in 12.9 seconds, after which the speed of straightening the wheels decreases to zero until the exit of the curve. The situation repeats itself after entering a curve with a radius of R = 3 [m], except that the maximum steering angle is smaller, at - 0.236 [rad], and is reached at 26.9 in a second of driving. The speed of turning and straightening of the wheel, due to the higher driving speed, reaches higher values of 0.177 [rad/s] in 22.8 seconds and 0.181 [rad/s] respectively in 27.4 seconds of driving.

Figure 6d, shows how the angular velocities of the individual wheels of the mobile robot *2, 3, 4* change during the movement. When driving along a straight section within five seconds of the start of movement, the characteristic point A accelerates from 0 to 0.5 [m/s] and thus the angular velocity of all wheels of the robot increases linearly from a value of 0 to 3.33 [rad/s]. Then, for a period of one second, the robot moves in a uniform rectilinear motion, and there is no change in the angular velocity of the wheels. After entering a curve with a radius of

R = 2 [m], the robot's motion speed is kept constant, but each of the three wheels begins to move along a different motion trajectory, and thus the angular velocity values of the individual wheels change. Driving wheel 2 moves along the inner trajectory, so it travels the shortest distance in the same interval and its angular velocity decreases. While moving around a curve, it reaches its lowest value in the 12th second of movement, equal to 2.72 [rad/s]. Driving wheel 3 moves on the outer track of motion, so it travels the longest distance in the same time interval and its angular velocity increases, reaching a maximum value of 3.95 [rad/s] in the 12th second of motion. Torsion wheel 4 follows a trajectory approximately coinciding with the trajectory of characteristic point *E*, so its angular velocity also increases and at the 12th second of movement is 3.55 [rad/s]. After exiting the turn, the robot moves in a uniform rectilinear motion and then, from 18.5 seconds to 21.5 seconds after the start of the simulation, it accelerates. Characteristic point *A* of the robot accelerates from 0.5 [m/s] to a speed of 1.0 [m/s], the angular velocity of rotation of its own all wheels increases linearly and reaches a value of 6.66 [rad/s]. At 22.4 seconds from the start of travel, the robot enters an arc with a radius of R = 3 [m] at a speed of 1 [m/s]. This speed does not change while driving around the curve, while – similar to driving around the curve with a radius of R = 2 [m], the angular velocities of the individual wheels change. Driving wheel 2 moves on the outer track this time, and its angular velocity decreases. As it moves around the bend, it reaches its highest value, equal to 7.47 [rad/s] at 26.9 seconds of movement. Driving wheel 3 moves along the inner track of motion, so its angular velocity decreases and reaches its smallest value of 5.86 [rad/s] at 26.9 seconds of motion. Torsion wheel 4 moves along a trajectory that approximately coincides with the trajectory of the characteristic point *E*, so its angular velocity increases; at 26.9 seconds of movement it is 6,86 [rad/s].

10. SIMULATION RESULTS FOR THE TWO-WHEELED ROBOT KINEMATICS

Simulation results for the model describing the kinematics of the two-wheeled mobile robot are shown in Figure 7.

Figure 7a shows the change in the instantaneous angle of rotation of the characteristic point E – β and its angular velocity – $\dot{\beta}$. During the simulations, models of two types of two-wheeled and three-wheeled mobile robot in motion along the same trajectory were studied, and it was noted that the course of changes in the described parameters (i.e., the change in the instantaneous angle and angular velocity of the rotation of the characteristic point *E*), is analogous in both cases.

Figure 7b illustrates how the angle of instantaneous rotation of the frame 1 – γ and its angular velocity – $\dot{\gamma}$ changes during the analysed movement of the two-wheeled robot. Clear differences can be seen in the course of changes in the value of

the maximum angular velocity of the two-wheeled robot and the three-wheeled robot. Thus, when driving the two-wheeled robot along an arc with a radius of $R = 2$ [m], we already reach a maximum value of 0.251 [rad/s] in the 9th second after the start of the simulation. It is also noteworthy that this value of velocity is maintained for 3.2 seconds and only at 12.3 seconds of driving does it begin to decrease, with the process of reducing the angular velocity to zero taking place in a short time – rapidly. The same is true when driving around a curve with a radius of $R = 3$ [m]. The angular velocity of the frame reaches a maximum value in a short time. At 25.5 seconds of the simulation, it reaches a value of 0.334 [rad/s], and then maintains this value until 28.5 seconds of driving.

A comparison of the curves in Figures 6b and 7b, which show, among other things, the change in the angular velocity of the frame of the three-wheeled and two-wheeled robot, respectively, shows significant differences:

- the maximum angular velocity values are different when driving on curves with the same radii and at the same value of the speed of the characteristic point *A*;
- in the case of the two-wheeled robot, there is an "abrupt" rise and fall of the angular velocity of the frame;
- in the two-wheeled robot, there is almosty a three-second period of constant angular velocity of the frame during the arc;
- in a two-wheeled robot, there is a relatively smooth transition from the period of increase in angular velocity to the period of constant angular velocity and from the period of constant angular velocity to the period of decrease in frame angular velocity;
- there is less "smoothness" in the curves representing the change in angular velocity of the frame of a two-wheeled robot than for a three-wheeled robot.

Figure 7c shows how the angular velocities of the two-wheeled mobile robot's driving wheels 2, 3 and trailing wheel 4 change during movement, for ease of analysis of the angular velocity of the two-wheeled robot's frame.

For the same reason, the values of the angular velocities of the driving wheels are doubled in the diagram, and the frame angular velocity values are 10 times the actual values. The speed of trailing wheel 4 is greater than that of driving wheels 2 and 3 primarily because the diameter of the driving wheels is three times that of the trailing wheel.

Comparison of the curves in Figures 6d and 7c, which show, among other things, the change in the angular velocity of the wheels of the three-wheeled and two-wheeled robots, respectively, show no significant differences when the robots are driving along rectilinear sections.

The analysis of the change in the angular velocity of the wheels when driving on a curve allows us to draw analogous conclusions as when analysing the graphs in Figures 6b and 7b.

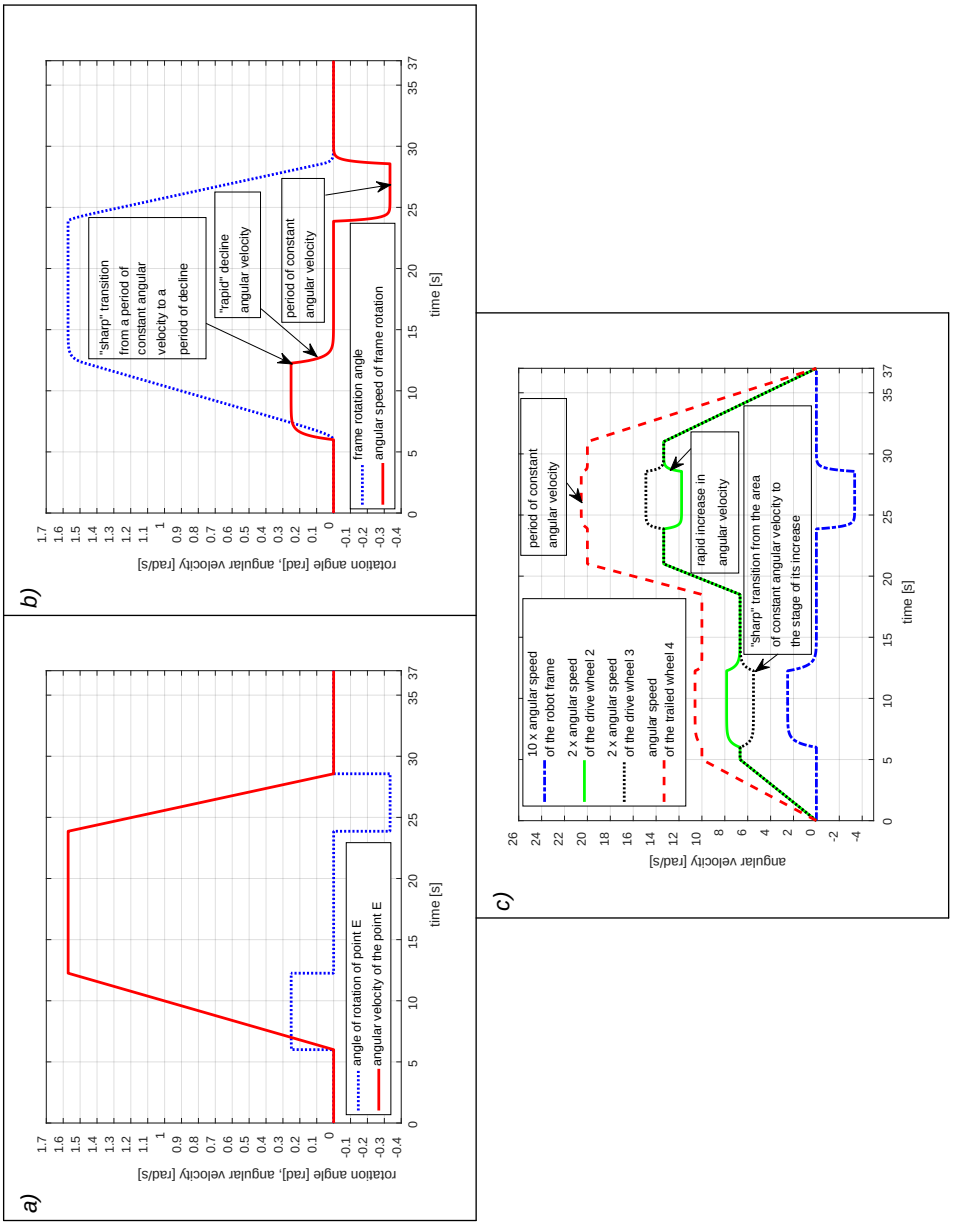

Fig. 7. Simulation results of the kinematic model of a two-wheeled robot: a) changing the instantaneous rotation angle and angular velocity of the robot's characteristic point *E*, b) change in the instantaneous rotation angle of the robot frame and its instantaneous angular velocity, c) changes in the angular speeds of the robot's wheels and frame

Source: own elaboration.

Differences in the course of the given motion parameters during curved driving are due to, among other things:

- the fact that in the case of a three-wheeled robot the characteristic point E is associated with steering wheel 5, which is twisted by angle ϕ. The value of the steering wheel twist angle continuously affects the course of changes in the steering angle of the frame 1 and the angular velocities of wheels 2, 3 and 4;
- different geometry of the systems analysed (for example, in the case of a three-wheeled robot, the distance between the characteristic point A and the characteristic point E is more than 3 times greater than in the case of a two-wheeled robot).

The demonstrated differences significantly affect the usefulness of the derived kinematic models. Knowledge of the parameters describing the robot's kinematics is essential for solving the robot's dynamics, in particular for calculating angular accelerations. In the case of a three-wheeled robot, the curves describing angular velocities are sufficiently "smooth." There are also no places where for one value of time there is more than one value of the described parameter. Determining the changes in the derivatives of these parameters does not pose major problems. The analysed model of the kinematics of the two-wheeled robot does not give confidence in the correctness of the obtained graphs of changes in the derivatives of individual parameters when the robot enters and leaves the arc.

In practice, the changes in the derivatives of the described parameters during entering and leaving the arc, obtained during the simulation of the dynamics model, show significant errors. The value of these errors is several hundred times greater than the value of the "correct" signal. The kinematics model of the two-wheeled robot is correct, but before using the obtained results in solving the dynamics model, it is necessary to approximate the angular velocity waveforms obtained in the transient periods with appropriately selected analytical functions. Only such angular velocity results can be used in solving the dynamics problem of a mobile two-wheeled robot.

11. SIMULATION RESULTS FOR THE THREE-WHEELED ROBOT DYNAMICS

Simulation results for the model describing the dynamics of the three-wheeled mobile robot, are shown in Figure 8.

Figure 8a shows the time course of the change in the driving torque M_{NS}, which is transferred from the motor via a gearbox with a ratio i_N to the driving wheel 2z so that the robot moves at a certain speed. For the first 5 seconds of travel, when the robot moves along a rectilinear section and accelerates from 0 [m/s] to 0.5 [m/s], the necessary torque that must be generated in the motor is 3.74 [Nm]. Between 5 and 6 seconds the robot moves at a constant speed of v_A = 0.5 [m/s], and the torque

generated by the motor is 3,39 [Nm]. After entering a turn with a radius of $R = 2$ [m], there is a continuous change in the value of the torque. First, the torque increases from 3.39 [Nm] to 3.52 [Nm], then as wheel 4 begins to straighten, the torque generated by the engine decreases to a value of 3.29 [Nm] and again increases so that, when exiting the turn, the torque on the engine is 3.39 [Nm]. After leaving on a straight section of movement, the value of the torque increases to a value of 3.97 [Nm], due to the acceleration of the robot from a speed of 0.5 [m/s] to 1 [m/s]. After reaching the required speed, the robot moves at a constant speed of 1 [m/s] and then the torque is again 3,39 [Nm]. After entering a curve with a radius of R =3 [m], at a constant speed, the moment first decreases to a value of 3.15 [Nm] and then increases to a value of 3.64 [Nm], after which it decreases and is again 3.39 [Nm] when exiting the curve. During speed extinction from 1 [m/s] to 0 [Nm], the torque is 2.92 [Nm]. From the analysis presented, it can be seen that the effect of the robot's moving speed v_A on the value of the driving torque is greatest during the acceleration of the robot. When driving the robot along a straight section, at a constant speed, the driving torque is constant (regardless of the value of the speed at which the robot is moving). When driving, along a curve at a constant speed, the changes in driving torque are smaller than when accelerating to a given speed value.

The change in Lagrange multipliers during driving is shown in Figure 8b, they have a physical interpretation, as the components of dry friction forces occurring in the plane of contact between the substitute wheel and the roadway Determination of Lagrange multipliers, allowed to determine the values of friction forces on substitute wheel 2*z* and torsion wheel 4.

Figure 8c shows the change in the value of the friction force on substitute wheel 2*z*. The solid line shows the value of the boundary friction force of 1024.2 [N]. In the event that the resultant frictional force T_{Hz} (dashed line in Fig. 8c) exceeded this value, the assumption of no slippage in the system would not be valid. In the event that such a situation occurred during acceleration of the vehicle to a certain speed, this could be an important signal to limit the maximum speed of circular movement of the mobile robot to a value at which the no-slip assumption is true. In the system analysed, the maximum frictional force on the substitute wheel was 971 [N] and occurred during curved travel. Figure 8c also shows the change in the value of the circumferential component of frictional force T_{OHz} (dotted line) and the transverse component of frictional force T_{PHz} (dashed dotted line) on the substitute wheel during driving.

Figure 8d shows the change in the value of the frictional force on torsion wheel 4. The solid line shows the value of the limiting frictional force of 1008,5 [N]. In the event that the resultant frictional force T_K (marked with a dashed line in the figure) exceeded this value, then the assumption of no slippage in the system would not be true at the assumed motion speeds of the robot or the assumed friction coefficients.

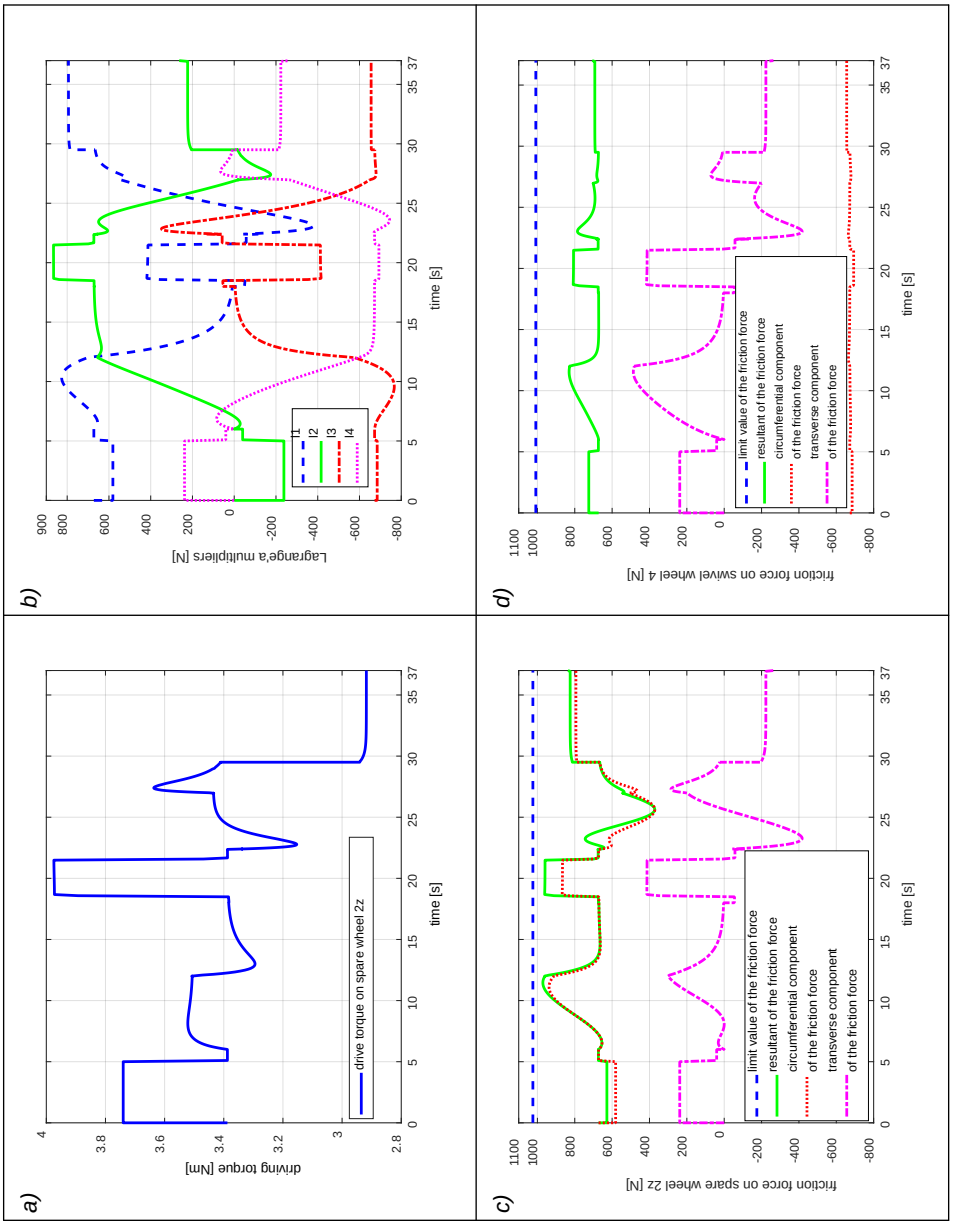

Fig. 8. Simulation results of a dynamic model of a three-wheeled robot*:* a) changes in the M_{NS} driving torque on the replacement 2*z* drive wheel, b) change of *Lagrange'a* multipliers (components of dry friction forces occurring in the plane of contact of robot wheels), c) change in the value of friction forces on replacement wheel 2*z*, d) change in the value of friction forces on steering wheel 4

Source: own elaboration.

If such a situation occurred, it would be a signal to limit the maximum movement speed to such a value, at which the assumption of no slippage is true, or to change the materials from which the driving wheels were made (to those characterised by other coefficients of friction), or to limit the type of substrates on which the robot could move. In the system analysed, the maximum frictional force on the torsion wheel was 808 [N] and occurred during the curved travel.

Figure 8d also shows the change in the value of the circumferential component of frictional force T_{OK} (dotted line) and the transverse component of frictional force T_{PK} (dashed dotted line) on torsion wheel 4 during driving.

Comparing with each other the nature of changes in frictional forces on substitute wheel *2z* and torsion wheel 4, it should be noted that the transverse component has a much greater effect on the value and course of the resultant frictional force on the torsion wheel than on the substitute wheel.

12. CONCLUSIONS

This paper presents a methodology for the construction of computational models describing the kinematics and dynamics of wheeled mobile robots while traveling along a specified trajectory. Based on the specified principles, appropriate models were derived for a three-wheeled robot and then their computer simulation was carried out.

Based on the achieved simulation results, the suitability of the computational model for the design of the drive and actuation systems of a wheeled mobile robot was demonstrated. The obtained waveforms of variation of the parameters analysed during motion can also be helpful in synthesising algorithms for controlling the tracking motion of a three-wheeled robot.

The methodology used in this paper for describing the kinematics and dynamics of mobile robots always yields correct solutions when determining the differential equations of motion of robots that have a steering system consisting of motor(s), steering wheel(s) and torsion wheel(s). Then, regardless of the number of wheels of the robot, an alternate model can be created, consisting of one driving wheel and one torsion wheel. Changing the direction of motion in such robots is mainly done by turning the steering wheel.

Using the example of analysis of a model describing the kinematics of a two-wheeled robot Pioneer 2-DX, in which the change of direction is carried out by means of the control system of the speed of the driving wheels, the reasons are given why the methodology presented in the paper does not make it possible to obtain satisfactory results when laying out the dynamics model without prior approximation (e.g. higher derivatives with appropriate analytical functions).

REFERENCES

Giergiel, J., Hendzel, Z., Żylski, W., 2013, *Modelowanie i sterowanie mobilnych robotów kołowych*, Wydawnictwa Naukowe PWN, Warszawa.

Jasiński, K., 2004, *Analiza oraz symulacja kinematyki i dynamiki nieholonomicznego robota mobilnego*, praca magisterska, Politechnika Gdańska, Katedra Mechaniki i Wytrzymałości Materiałów, (maszynopis).

Kaliński, K.J., Mazur, M., 2016a, *Optimal Control at Energy Performance Index of the Mobile Robots Following Dynamically Created Trajectories*, Mechatronics, vol. 37, p. 79–88.

Kaliński, K.J., Mazur, M., 2016b, *Optimal Control of 2-Wheeled Mobile Robot at Energy Performance Index*, Mechanical Systems and Signal Processing, vol. 70–71, pp. 373–386.

Mazur, M., 2010, *Nadzorowanie ruchu 2-kołowej platformy mobilnej z zastosowaniem sterowania optymalnego przy energetycznym wskaźniku jakości*, rozprawa doktorska, Politechnika Gdańska, Wydział Mechaniczny (maszynopis).

Żylski, W., 1996, *Kinematyka i dynamika mobilnych robotów kołowych*, rozprawa habilitacyjna, Oficyna Wydawnicza Politechniki Rzeszowskiej, Rzeszów.